

Size-selective colloidal-gold localization in transmission X-ray microscopy

H. STOLLBERG, P. GUTTMANN*, P. A. C. TAKMAN
& H. M. HERTZ

Biomedical and X-Ray Physics/Department of Applied Physics, KTH-AlbaNova, 10691 Stockholm, Sweden

*Institut für Röntgenphysik, Georg-August-Universität Göttingen, c/o BESSY, 12489 Berlin, Germany

Key words. colloidal gold, image analysis, soft X-ray microscopy.

Summary

Colloidal gold is a useful marker for functional-imaging experiments in transmission X-ray microscopy. Due to the low contrast of gold particles with small diameters it is necessary to develop a powerful algorithm to localize the single gold particles. The presented image-analysis algorithm for identifying colloidal gold particles is based on the combination of a threshold with respect to the local absorption and shape discrimination, realized by fitting a Gaussian profile to the identified regions of interest. The shape discrimination provides the possibility of size-selective identification and localization of single colloidal gold particles down to a diameter of 50 nm. The image-analysis algorithm, therefore, has potential for localization studies of several proteins simultaneously and for localization of fiducial markers in X-ray tomography.

Introduction

X-ray microscopy allows high-resolution imaging of thick biological structures with natural contrast. Functional imaging requires high-spatial-resolution localization of specific proteins. In X-ray microscopy, colloidal gold is a suitable marker due to its strong absorption. In this paper we present an image-analysis algorithm that size-selectively can detect single colloidal gold particles in transmission X-ray microscope (TXM) images, aiming towards high-resolution localization studies.

Immunolabelling is an established method for localization of proteins in cells both in light microscopy and electron

microscopy. Fluorescence microscopy allows studies of dye-labelled proteins in living cells. Several proteins can be studied simultaneously by double labelling, i.e. different proteins are tagged with different fluorophores in combination with a multicolour detection. One important field of application are colocalization studies of proteins. In electron microscopy, immunogold labelling has been a standard method for many years (Faulk & Taylor, 1971; Roth, 1983). Both colloidal gold and silver-enhanced colloidal gold markers of different sizes are used. Double-labelling experiments based both on size selectivity and element selectivity have been described for electron microscopy (Roth & Binder, 1978; Roth, 1983). In electron microscopy the resolution is high and the diameter of a colloidal gold particle in the image often covers 10 or more resolution elements. In this case standard pattern recognition methods as described in Gonzales & Woods (2002) can be used.

Soft X-ray microscopy in the water-window region ($\lambda = 2.3\text{--}4.4$ nm) is an attractive technique for high-resolution biological imaging owing to the possibility of studying thick unstained objects (Schmahl *et al.*, 1980; Kirz *et al.*, 1995). Such microscopes rely on the natural contrast between water and, e.g. carbon-containing material. Soft X-ray microscopy allows imaging of whole hydrated or cryo-fixed cells with a resolution of a few tens of nanometres and can, therefore, fill a gap between electron microscopy and light microscopy applications. However, only a few experiments have been published on functional imaging. A theoretical approach to use colloidal gold as a marker for scanning X-ray microscopy was developed by Chapman and colleagues (Chapman *et al.*, 1996a) and demonstrated on fibroblast cells where tubulin was labelled with gold (Chapman *et al.*, 1996b). In transmission X-ray microscopy colloidal gold has been used to determine the presence of certain proteins (Vogt *et al.*, 2000) and to visualize microtubule networks (Meyer-Ilse *et al.*, 2001). In both cases

an intensity threshold was used to obtain overview information about the protein localization.

In the present paper we describe an image-analysis algorithm to determine the specific position of single colloidal gold particles in TXM images. Furthermore, we investigate the potential for size selectivity in samples double labelled with gold particles of different diameters. The major issue is the limited contrast and, thus, low signal-to-noise ratio for small-diameter gold particles. The algorithm has potential applications in high-resolution localization studies of several proteins simultaneously, colocalization studies, and localization of fiducial markers in tomography.

Experimental arrangement

X-ray microscopes

To develop and optimize the algorithm, images were recorded with the TXM at BESSY II in Berlin. The instrument is located at an undulator beam line. The rotating condenser system is adapted to the highly collimated X-ray beam of the undulator and can match the numerical aperture of any micro objective zone plate (Niemann *et al.*, 2000). The actual arrangement of the TXM (Guttman *et al.*, 2003) is using a micro zone plate with 25-nm outermost zone width. No object structures with spatial frequencies higher than the cut-off frequency of the optical system will be transferred (Vogt *et al.*, 2000). The cut-off frequency derived for the actual set-up corresponds to smallest feature sizes of 19.5 nm. The images used for the present study were taken at a wavelength $\lambda = 2.36$ nm. The pixel size in the object plane was 9.8×9.8 nm². Besides the BESSY II images, images recorded with the compact X-ray microscope at KTH in Stockholm (Takman *et al.*, 2006,) at a wavelength of $\lambda = 2.48$ nm were used to test the performance of the algorithm.

Specimen preparation

The test samples were dry specimens containing both cell-like structure and colloidal gold particles. Diatoms were chosen as cell-like structures. The diatoms from the Experimental Phycology and Culture Collection of Algae (Göttingen/Germany) were suspended in distilled water. This solution was mixed with monodispersed suspensions of colloidal gold particles in distilled water from BBInternational (Cardiff, U.K.). The mean diameters of the chosen colloidal gold particles were 39.9, 50, 80.8, 100.7 and 154.1 nm according to the manufacturer, all with a standard deviation in size of 8%. The final mixture was dropped on a silicon nitride membrane and let dry. The samples contained either one size of gold particles or a mixture of two different sizes.

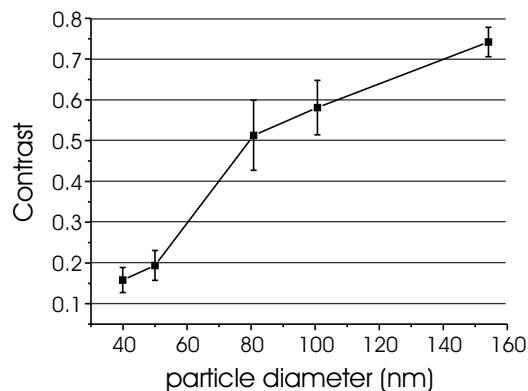


Fig. 1. Contrast for gold particles at the BESSY II transmission X-ray microscope.

Colloidal-gold contrast

The recorded effective absorption in the TXM is size-dependent due to the spatial-frequency dependence of the microscope's modulation transfer function. The contrast of the gold particles was determined by evaluating experimental images with gold particles of different sizes and different exposure times. The contrast for a number of colloidal gold particles inside and outside the background structure was calculated by comparing the transmitted intensity in the background to the transmitted intensity of the gold particles, normalizing the transmission of the surrounding environment to 1. The contrast can then be calculated by

$$\text{Contrast} = \frac{1 - T_{\text{Au}}}{1 + T_{\text{Au}}}, \quad (1)$$

where T_{Au} is the relative transmission of the gold particles compared to the background.

Figure 1 shows the contrast of gold particles for the BESSY II TXM.

Image analysis

In order to develop, optimize and evaluate the image-analysis algorithm for size-selective identification and localization of single gold particles, images containing colloidal gold particles of different sizes and different background structures were used. These images were taken with the TXM at BESSY II.

Figure 2 shows an overview of the algorithm. In brief, the algorithm combines local absorption thresholding with discrimination due to shape. The goal is to identify the position of as many gold particles as possible and to minimize at the same time the number of false identifications arising from noise in the low-signal, varying background images. In the following the steps are described in more detail. Figure 4 in the end of this section shows the major steps of the image-analysis algorithm on a real image.

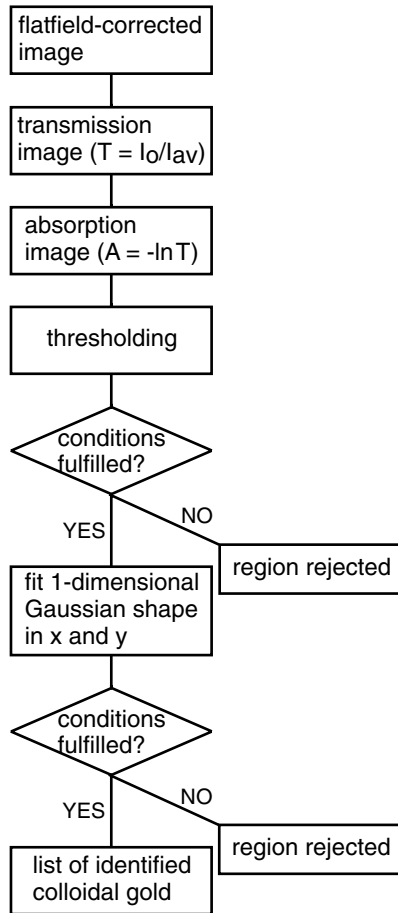


Fig. 2. Flow chart of the image-analysis algorithm to localize single colloidal gold particles in X-ray microscope images.

Absorption image

After dark-field subtraction and flat-field correction, the local transmission image T is calculated via

$$T = \frac{I_0}{I_{av}}, \quad (2)$$

where I_0 is the intensity value in a pixel and I_{av} is the average intensity value in the pixel's immediate surrounding. This operation smoothes larger structures while high-frequency components of the image, like the colloidal gold particles, are enhanced. The transmission image is then transformed into an absorption image A according to

$$A = -\ln T \quad (3)$$

The local-transmission image T is calculated by the use of a surrounding frame (I_{av}), as shown Fig. 3. This square frame is moved pixel-by-pixel over the whole image. The optimum size of this surrounding frame was determined by comparing the intensity distributions in several original images with their respective transmission image. A surrounding frame with a width of four times the radius of the colloidal gold

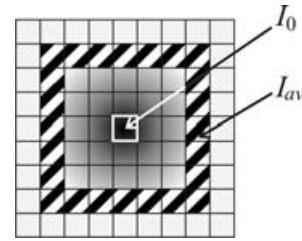


Fig. 3. The calculation of the transmission value of a pixel is done by dividing the intensity (I_0) of the pixel with the averaged intensity (I_{av}) in a surrounding square frame.

particles provides the optimum trade-off to maintain both the transmission value and the shape information as close to the original image as possible. For simplicity the size of the surrounding is kept constant for the image and not changed with the structural data. To reduce the execution time of the algorithm, a square frame is used.

Thresholding

A threshold is applied to the absorption image to identify the positions of potential colloidal gold particles. This step requires knowledge about the imaging properties of the microscope. To find an optimal threshold value, the colloidal-gold contrast of the microscope (Fig. 1) is employed. The average absorption value for a gold particle of known size can then be calculated.

The absorption image is searched in square regions with a side length of two times the diameter of the colloidal gold particles. When the maximum pixel intensity in a region is above the chosen threshold, the square region is centred on this pixel. Again, the pixel with the maximum intensity value is identified and the surrounding is centred once more. This procedure is repeated until the pixel with maximum intensity value lies in the centre of the square. The region is then marked as a potential gold particle. The thresholding continues until the whole image has been searched. With this search algorithm it is possible for the found regions to overlap each other. A lower threshold value of about 70% of the average absorption value according to the determined contrast (Fig. 1) typically allows more than 95% of the particles to be identified. Unfortunately, the cell-like structures can have absorption similar to gold particles, and might be falsely identified as colloidal gold particles. The same is true for noise and defect pixels. To limit the number of false identifications, the maximum absorption value for every detected region has to be below 130% of the average absorption value of the colloidal gold particles. In the 70–130% interval more than 90% of the colloidal gold particles can be found and the number of false identifications due to noise or defect pixels is reduced. However, there are still many falsely identified regions, especially if the absorption of the colloidal gold particles differs only slightly from the absorption of the background structure. The use of only thresholding

is, therefore, often not sufficient to unambiguously identify colloidal gold particles in an X-ray microscope image.

Shape discrimination by Gaussian fit

In order to reduce the number of false identifications, the shape of the potential gold particles identified by thresholding is determined by a Gaussian fitting procedure. Due to the known size of the colloidal gold particles this provides an effective discrimination via size and shape criteria. A Gaussian shape proved superior to other possible shapes for these high-noise few-pixel absorption profiles. We fit the profiles of the pre-identified region to two perpendicular one-dimensional (1D) Gaussians. This method proved less noise-sensitive than the fitting of an elliptical two-dimensional (2D) Gaussian shape.

Using a least-square fit on the regions around the potential gold particles in the absorption image, the particles are described as Gaussian functions in both the x - and y -directions according to

$$\begin{aligned} A_x &= A_{m,x} e^{-\left(\frac{x-x_0}{w_x}\right)^2} + A_{\text{offset},x}; \\ A_y &= A_{m,y} e^{-\left(\frac{y-y_0}{w_y}\right)^2} + A_{\text{offset},y}. \end{aligned} \quad (4)$$

The parameters to describe the 1D Gaussian distributions are the peak positions (x_0 or y_0 , respectively), the maximum absorption ($A_{m,x}$ or $A_{m,y}$, respectively) and the $1/e$ -radius (w_x or w_y , respectively). The offset in absorption (A_{offset}) is close to zero and, therefore, neglected. The nominal radius of the colloidal gold particles and the average absorption according to the contrast curve (Fig. 1) are chosen as initial values for the fit procedure.

The lateral extension for the Gaussian fit is chosen to be ± 1.5 times the diameter of the colloidal gold particle. The interval depends only on the size of the colloidal gold and is

kept constant throughout the procedure. This optimal interval was determined from a comparison of the number of rightly and falsely identified particles. A larger interval proves difficult for particles embedded in a fine structure; a smaller interval gives too many false fits. The resolution of the algorithm to find colloidal gold particles close to each other depends on the interval size.

The conditions used in the shape-discrimination step of the algorithm are summarized in Table 1. To exclude false identifications due to noise or structure, the conditions of Table 1 for the centre coordinates (x_0 , y_0), the $1/e$ -radius (w) and the maximum value (A_m) of the Gaussian shapes have to be fulfilled. To further increase the efficiency of the algorithm and decrease the number of falsely identified particles, the following additional conditions are employed:

- 1 The absolute residual errors (Err_{1D} , Err_{2D}) between the 1D absorption profiles ($profile_{1D}$) and the 1D Gaussian shapes, as well as between the original 2D absorption profile ($profile_{2D}$) and the elliptical Gaussian shape,

$$A = \frac{A_{m,x} + A_{m,y}}{2} \exp\left(\frac{(x-x_0)^2}{w_x^2} + \frac{(y-y_0)^2}{w_y^2}\right), \quad (5)$$

are restricted (for exact values see Table 1). All parameters in Eq. (5) are determined by the 1D Gaussian fits in x - and y -direction, respectively.

- 2 The ratio between the absolute maximum value of the residual (δ_{1D} , δ_{2D}) and the average absorption value of colloidal gold according to the contrast curve (Fig. 1) (A_{collAu}) is limited (see Table 1).
- 3 The ratio of the integrated absorption ($A_{\text{tot},2D}$) and the average absorption value (A_{collAu}) is restricted (see Table 1).

The output of the algorithm is a list with the centre coordinates of all regions identified as colloidal gold particles.

Table 1. All conditions that the one-dimensional Gaussian fits and the resulting two-dimensional Gaussian shape have to fulfil are listed. The absolute values of the parameters have been evaluated by manual inspection of the result of the image analysis for images with both 80- and 50-nm colloidal gold particles and different background structure. x_{max} , y_{max} : coordinates of maximum value; d : particle diameter in pixel; A_{collAu} : average absorption of the gold particles, calculated with the contrast as shown in Fig. 1 and $\#pixel$: number of pixels in the 1D or 2D absorption profile.

Fit parameter		Condition to be fulfilled
Peak coordinates	x_0, y_0	$x_{\text{max}} - 1.5 d < x_0 < x_{\text{max}} + 1.5 d$ $y_{\text{max}} - 1.5 d < y_0 < y_{\text{max}} + 1.5 d$
Peak value	$A_{m,x}, A_{m,y}$	$0.6 A_{\text{collAu}} < A_{m,x}, A_{m,y} < 1.2 A_{\text{collAu}}$
$1/e$ -radius	w_x, w_y	$0.4 d < w_x, w_y < 0.95 d$
Residual error (1D and 2D)	$Err_{1D} = \sum profile_{1D} - \text{Gaussian}_{1D} $ $Err_{2D} = \sum_x \sum_y profile_{2D} - \text{Gaussian}_{2D} $	$Err_{1D}, Err_{2D} < 0.14 \times \#pixel$
Maximum deviation value of the 1D residual	$\delta_{1D} = \max(profile_{1D} - \text{Gaussian}_{1D})$	$\delta_{1D} < 0.8 A_{\text{collAu}}$
Maximum deviation value of the 2D residual	$\delta_{2D} = \max(profile_{2D} - \text{Gaussian}_{2D})$	$\delta_{2D} < 0.9 A_{\text{collAu}}$
2D integrated absorption	$A_{\text{tot},2D} = \sum_x \sum_y profile_{2D}$	$A_{\text{tot},2D} < 0.36 A_{\text{collAu}} \times \#pixel$

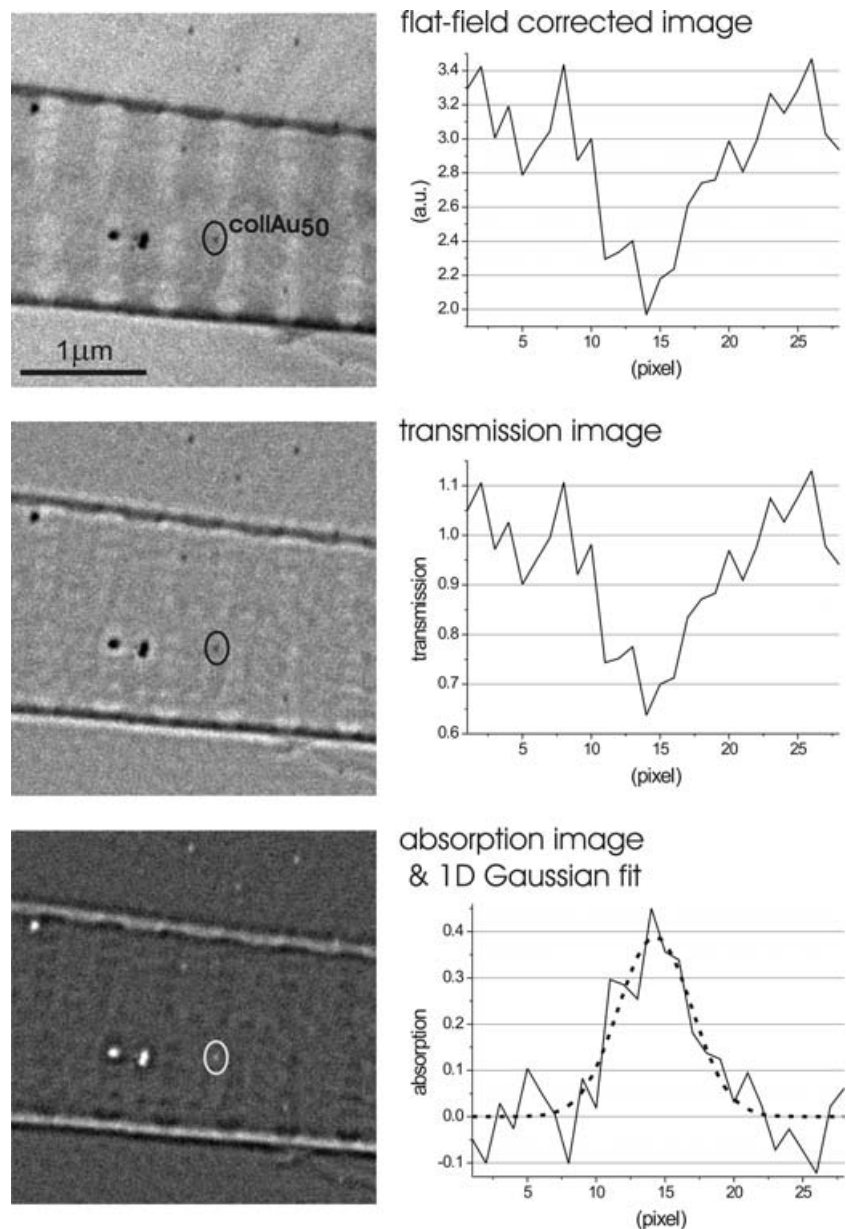


Fig. 4. The steps of the image-analysis algorithm. On the left, a part of an image with an elongate diatom and 50-nm and 80-nm gold particles is shown. On the right a profile through one of the 50-nm gold particles is depicted. The upper left image is the flat-field corrected image. In the next step the transmission image is calculated (middle left). Every pixel gets a relative transmission value with respect to its surrounding. Thereafter the absorption image (lower left) is calculated according to Eq. (3). In the last step a one-dimensional Gaussian shape is fitted to the profile (lower right, dotted line).

The steps of the algorithm are shown in Fig. 4. Here the algorithm is applied to one 50-nm gold particle in an image containing 50- and 80-nm gold particles and an elongate diatom as background structure.

Discussion and conclusions

The goal of the algorithm is to size-selectively identify single colloidal gold particles inside and outside cell-like structures. Images with smaller (diameter = 50 nm, corresponding to 5 pixels) and larger (diameter = 80 nm, corresponding to 8 pixels) colloidal gold particles and different background structure (round and elongate diatoms) were used to optimize the algorithm.

Diatoms were chosen since they resemble cells and provide a reproducible means to develop and evaluate the algorithm. Diatoms are eukaryotic algae with cell walls made of silicate, which show structures sized from several micrometers down to a few nanometers. The integrated absorption in the diatoms is similar to or higher than the integrated absorption of typical cells. Furthermore, the absorption of diatoms is higher than the absorption of a typical layer of water or vitreous ice. Diatoms are, therefore, used as a model for cells in this project. In addition, diatoms may show regular pores equivalent in size to that of the colloidal gold particles, which makes the identification of the gold particles more demanding.

The performance of the algorithm depends on both the absorption and the size of the colloidal gold particles. In case

Table 2. The algorithm was evaluated on a several BESSY II TXM images with different diameters of the colloidal gold particles, different background structure and different noise levels. The columns include (left to right): The nominal diameter of the particle and the corresponding diameter in pixels; the background structure; the signal-to-noise ratio of colloidal gold particles in the absorption image; the number of images used for the analysis ('# images'); the total number of gold particles in these images as determined by manual counting ('# gold particles'); the total number of gold particles found by thresholding ('# found by thresholding: total (correct)') out of which a number ('correct', in parenthesis) were correctly identified; the number of correctly found particles after the fitting procedure ('# found by fit procedure') and finally the number of erroneously identified particles ('# false identifications').

Particle diameter		Background structure	Signal-to-noise ratio	# images	# gold particles	# found by thresholding: total (correct)	# found by fit procedure	# false identifications
(nm)	(pixel)							
40	4	Round diatom	7...8	3	35	1230 (31)	12	43
		Elongate diatom	7...8	2	29	771 (23)	10	21
50	5	Round diatom	5...8	3	58	1346 (54)	31	15
		Elongate diatom	6...9	4	71	1010 (64)	45	15
80	8		8...9*	2	28	326 (23)	21	4
		Round diatom	10...20	5	72	115 (68)	60	0
100	10	Elongate diatom	12...20	4	24	188 (24)	23	0
		Round diatom	11...25	9	137	599 (125)	98	0
		Elongate diatom	23	1	9	49 (9)	8	0

*Subset of data.

of low contrast, i.e. the absorption of the particles is close to the absorption of the surrounding structure, a minimum diameter of 5 pixels is needed to perform a well-adapted fit of a Gaussian shape to identify the gold particles correctly. For the magnification used in this study the algorithm, therefore, does not work sufficiently well for particles with a diameter of 40 nm (corresponding to 4 pixels). Too many structural details are then falsely identified as colloidal gold particles due to the low contrast of these small gold particles. For a diameter of 50 nm, where the absorption differs only slightly from the absorption of the diatom structure, the algorithm performs well. By improving the resolution the performance of the algorithm will improve also for the smaller gold particles.

In Table 2 the evaluation of the algorithm is summarized. Obviously larger particle diameters are more easily identified with less false identifications than smaller-diameter particles. Clearly, the number of false identifications increases with the level of noise and depends also on the background structure. As already mentioned, round diatoms may show regular pores in the same size range as the gold particles (Fig. 5). For low absorption and corresponding low contrast, as for 50- and 40-nm colloidal gold particles, the structure in between these pores are often identified as gold particles. For the 50-nm gold particles the performance of the algorithm improves strongly with increased signal-to-noise ratio as is evident by comparing row '50' in Table 2 (all signal-to-noise ratio) and a subset of data, marked with *, where only images with higher signal-to-noise ratio were taken into account. For low signal-to-noise ratio the unambiguous identification of 50- and 40-nm gold particles is difficult with the present experimental set-up. Many

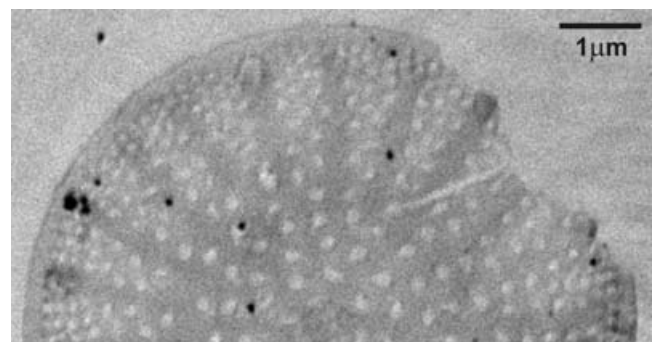


Fig. 5. A part of a round diatom with colloidal gold particles with a diameter of 50 nm and 80 nm. The pore structure of the diatom can clearly be seen. Close to the edges the pores get smaller and show structures similar to round particles.

of the falsely identified regions are due to noise and may afterwards be disregarded manually.

The inadequacy of only applying a threshold is clearly seen in Table 2. The number of false identifications for all sizes is much larger than the actual number of gold particles (Table 2, column '# found by thresholding'). The application of the shape-sensitive Gaussian fit is thus crucial to correctly identify single gold particles in X-ray microscope images.

To sum up, 100- and 80-nm particles are identified with high accuracy. For smaller particle diameter like 50 or 40 nm, the performance of the image-analysis algorithm depends strongly on the signal-to-noise ratio in the image.

When applying the algorithm to images taken by the Stockholm compact X-ray microscope (Takman *et al.*, 2006,

unpublished data), the image-analysis algorithm can be used without modification. The main differences between the compact microscope and the TXM at BESSY II are a larger pixel size in the object plane ($13 \times 13 \text{ nm}^2$) and a slightly lower contrast for the gold particles of the former. Both 100- and 80-nm gold particles can be identified with high accuracy. For the 50-nm colloidal gold particles the performance again depends strongly on the signal-to-noise ratio. The 40-nm gold particles cannot be imaged with sufficient contrast in the present compact microscope arrangement.

The size selectivity of the algorithm provides the possibility to perform double-labelling studies with differently sized particles, aiming at simultaneous localization of different proteins. With the conditions in Table 1 the algorithm is robustly size selective. This was tested by searching for 50- and 80-nm particles in samples containing particles of both sizes. In no case a particle of one size was identified as one of the other, even if the absorption value happened to be in the interval of the other size. The Gaussian-fit procedure thus provides strong size discrimination.

In immunolabelling experiments the colloidal gold should preferably be less than 10 nm in diameter to be incubated easily. Incubation with small gold particles and a subsequent silver size enhancement is a common technique (Holgate *et al.*, 1983; Burry *et al.*, 1992). In X-ray microscopy silver-enhanced particles of comparable size as the gold particles in the present study, have been used (Meyer-Ilse *et al.*, 2001). The attenuation lengths for gold and silver are similar within the water-window wavelength region above a photon energy of about 450 eV ($\lambda < 2.76 \text{ nm}$). Thus, for these wavelengths, the image-analysis algorithm is expected to work equally well on silver-enhanced colloidal gold as in the model experiments of this paper. For longer wavelengths the absorption of silver is smaller than that of gold, resulting in lower contrast and inferior algorithm performance.

Another field for application for the image-analysis algorithm may be X-ray tomography. Experiments on biological specimens have been performed in this field (Lehr, 1997; Weiß *et al.*, 2000), also in combination with colloidal-gold immunolabelling experiments (Schneider *et al.*, 2002; Larabell & Le Gros, 2004). Here the main purpose of the immunolabelling was the overview visualization of proteins, mainly by comparison to confocal laser scan micrograph images. Larger gold particles (100 nm) were used separately as fiducial markers for the tomography algorithm. With the image-analysis algorithm of the present paper one may use the same gold particles both for immunolabelling and as fiducial markers due to the accurately determined position of the single gold beads.

In summary, the image-analysis algorithm based on thresholding and shape discrimination has the potential to identify the precise localization of single colloidal-gold immunolabelled proteins in X-ray microscopy. The major

advantage compared to the threshold methods presently used is the accurate localization of single colloidal gold particles and the decreased number of falsely identified regions with a comparable absorption value. The strong size selectivity of the algorithm makes double-labelling experiments feasible.

Acknowledgements

The authors gratefully acknowledge the discussions with Linda Lundström. This work was financed by the Swedish Science Research Council.

References

- Burry, R.W., Vandr , D.D. & Hayes, D.M. (1992) Silver enhancement of gold antibody probes in pre-embedding electron microscopic immunocytochemistry. *J. Histochem. Cytochem.* **40**, 1849–1856.
- Chapman, H.N., Jacobsen, C. & Williams, S. (1996a) A characterisation of dark-field imaging of colloidal gold labels in a scanning transmission X-ray microscope. *Ultramicroscopy* **62**, 191–213.
- Chapman, H.N., Fu, J., Jacobsen, C. & Williams, S. (1996b) Dark-field X-ray microscopy of immuno-labeled cells. *J. Microsc. Soc. Am.* **2**, 53–62.
- Faulk, W.P. & Taylor, G.M. (1971) An immunocolloid method for the electron microscope. *Immunochemistry* **8**, 1081–1083.
- Gonzalez, R.C. & Woods, R.E. (2002) *Digital Image Processing*. Prentice Hall, Upper Saddle River, New Jersey.
- Guttman, P., Niemann, B., Rehbein, S., Kn chel, C., Rudolph, D. & Schmahl, G. (2003) The transmission X-ray microscope at BESSY II. *J. Phys. IV France* **104**, 85–90.
- Holgate, C.S., Jackson, P., Cowen, P.N. & Bird, C.B. (1983) Immunogold-silver staining: new method of immunostaining with enhanced sensitivity. *J. Histochem. Cytochem.* **31**(7), 938–944.
- Kirz, J., Jacobsen, C. & Howells, M. (1995) Soft X-ray microscopes and their biological applications. *Q. Rev. Biophys.* **28**(1), 33–130.
- Larabell, C.A. & Le Gros, M. (2004) X-ray tomography generates 3-D reconstructions of the yeast, *Saccharomyces cerevisiae*, at 60-nm resolution. *Mol. Biol. Cell* **15**, 957–962.
- Lehr, J. (1997) 3D X-ray microscopy: Tomographic imaging of mineral sheaths of bacteria *Leptothrix Ochracea* with the G ttingen x-ray microscope at BESSY. *Optik* **104**(4), 166–170.
- Meyer-Ilse, W., Hamamoto, D., Nair, A., *et al.* (2001) High resolution protein localization using soft X-ray microscopy. *J. Microsc.* **201**, 395–403.
- Niemann, B., Guttman, P., Hambach, D., Schneider, G., Weiß, D. & Schmahl, G. (2000) The condenser - monochromator with dynamical aperture synthesis for the TXM at an undulator beamline at BESSY II. *X-ray Microscopy* (ed. by W. Meyer-Ilse, T. Warwick and D. Attwood), Vol 507, pp. 440–445, AIP Conference Proceedings.
- Roth, J. & Binder, M. (1978) Colloidal gold, ferritin and peroxidase as markers for electron microscopic double labeling lectin techniques. *J. Histochem. Cytochem.* **26**, 960–966.
- Roth, J. (1983) The colloidal gold marker system for light and electron microscopic cytochemistry. *Techniques in Immunocytochemistry* (ed. by G.R. Bullock and P. Petrusz) vol. 2, pp. 217–284, Academic Press, London.
- Schmahl, G., Rudolph, D., Niemann, B. & Christ, O. (1980) Zone-plate X-ray microscopy. *Q. Rev. Biophys.* **13**(3), 297–315.

- Schneider, G., Anderson, E., Vogt, S., Knöchel, C., Weiss, D., Legros, M. & Larabell, C. (2002) Computed tomography of cryogenic cells. *Surf. Rev. Lett.* **9**(1), 177–183.
- Takman, P.A.C., Vogt, U. & Hertz, H.M. (2006) Towards compact x-ray microscopy with liquid-nitrogen-jet laser-plasma source. Proc. 8th Int. Conf. X-ray Microscopy (ed. by S. Aoki, Y. Kagoshima and Y. Suzuki), IPAP Conf. Series 7, Tokyo, 12–14.
- Vogt, S., Schneider, G., Steuernagel, A., Luchesi, J., Schulze, E., Rudolph, D. & Schmahl, G. (2000) X-Ray Microscopic Studies of the *Drosophila* Dosage Compensation Complex. *J. Struct. Biology* **132**, 123–132.
- Weiß, D., Schneider, G., Niemann, B., Guttman, P., Rudolph, D. & Schmahl, G. (2000) Computed tomography of cryogenic biological specimens based on X-ray microscopic images. *Ultramicroscopy* **84**, 185–197.